

Magnetic and Electronic Raman Scattering at the Nodal Spin-Density-Wave Transition in BaFe_2As_2

S. Sugai,^{1,2,3} Y. Mizuno,^{1,3} R. Watanabe,^{4,3} T. Kawaguchi,^{4,3} K. Takenaka,^{4,3} H. Ikuta,^{4,3} Y. Takayanagi,¹ N. Hayamizu,¹ and Y. Sone¹

¹Department of Physics, Faculty of Science, Nagoya University, Furo-cho, Chikusa-ku, Nagoya 464-8602, Japan

²Venture Business Laboratory, Nagoya University, Furo-cho, Chikusa-ku, Nagoya 464-8601, Japan

³TRIP, Japan Science and Technology Agency (JST), Chiyoda, Tokyo 102-0075, Japan

⁴Department of Crystalline Materials Science, Nagoya University, Furo-cho, Chikusa-ku, Nagoya 464-8603, Japan

(Dated: November 12, 2018)

Two magnon excitations and the nodal spin density wave (SDW) gap were observed in BaFe_2As_2 by Raman scattering. Below the SDW transition temperature (T_{SDW}) nodal SDW gap opens together with new excitations in reconstructed electronic states. The two-magnon peak remains above T_{SDW} and moreover the energy increases a little. The change from the long-range ordered state to the short-range correlated state is compared to the cuprate superconductors.

PACS numbers: 74.25.nd,74.70.Xa,75.30.Fv,75.30.Ds,75.40.-s

Iron pnictides form a new family of superconductors with the transition temperature up to $T_c = 55$ K [1, 2]. The superconductivity emerges as the spin density wave (SDW) is reduced by substituting an element or pressurizing. The stripe type spin order in the SDW state and the superconductivity are generally assumed to originate from the nesting of the hole Fermi surface (FS) at Γ and the electron FS at M [3–7]. The first issue is the change of the electronic states at the SDW transition, especially the SDW gap. If the SDW arises from the instability of itinerant electrons for the nesting, a gap opens at the FS. Ran *et al.* [8] predicted that the gap is not a full gap but a nodal gap. Infrared spectroscopy reported the SDW gap [9]. The present electronic Raman scattering disclosed opening of the gap in the (ab) and (xx) spectra, but not in (aa) and (xy) , indicating the nodal gap, were ($\hat{E}_i \hat{E}_s$) denotes that the electric fields of incident and scattered light are parallel to \hat{E}_i and \hat{E}_s . It is consistent with the very recent observation of the anisotropic gap observed in ARPES [10, 11]. The second issue is what kinds of exchange interactions work in the SDW state and what kinds of magnetic correlations remain above the SDW transition temperature (T_{SDW}). The two-magnon peak is observed at 2200 cm^{-1} in consistent with neutron scattering [12–16]. In order to explain the magnetic excitation spectra in metal a carrier hopping induced mechanism is proposed and compared to the cuprate superconductors.

BaFe_2As_2 undergoes the SDW state below $T_{\text{SDW}} = 137$ K [17, 18]. The crystal structure changes from tetragonal ($I4/mmm$) to orthorhombic ($Fmmm$) [17, 18]. The magnetic order in the SDW state is a stripe type in which nearest-neighbor spins are antiparallel in the x direction and parallel in the y direction [12–15, 19].

Single crystals of BaFe_2As_2 were grown by the self-flux method. Raman spectra were measured on the fresh cleaved surfaces in a quasi-back scattering configuration using 5145 \AA laser light. The crystallographic axes of the tetragonal structure are a and b and the bisecting

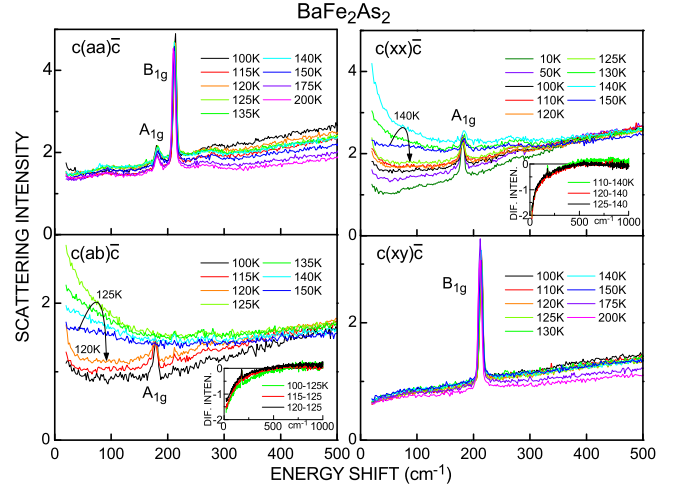


FIG. 1: (color online) Temperature dependent low-energy Raman spectra in BaFe_2As_2 . The $c(ab)\bar{c}$ and $c(xx)\bar{c}$ spectra show the SDW gap, but the $c(aa)\bar{c}$ and $c(xy)\bar{c}$ spectra do not show the gap. The insets are the differential spectra between below and above T_{SDW} .

directions are x and y . Raman active phonon modes are $1A_{1g} + 1B_{1g} + 2E_g$ in the tetragonal structure [20–23]. The A_{1g} , B_{1g} , and E_g modes change into the A_{1g} , B_{1g} , and $B_{2g} + B_{3g}$ modes in the orthorhombic structure, respectively. The (aa) spectra allow the $A_{1g} + B_{1g}$ ($A_{1g} + B_{1g}$) modes, (ab) no (A_{1g}) mode, (xx) $A_{1g} + B_{2g}$ (A_{1g}), and (xy) B_{1g} (B_{1g}) in the tetragonal (orthorhombic) structure. It should be noted that the crystallographic axes rotate by 45° as the structure changes from tetragonal to orthorhombic. The Raman system was calibrated so that the intensity is proportional to $\partial^2 S / \partial \omega \partial \Omega$.

The SDW gap is directly observed in the low-energy spectra in Fig. 1. In the (ab) and (xx) spectra the low energy part below 200 cm^{-1} increases as temperature decreases from 150 K and then abruptly decreases from

125 K to 120 K in (ab) and from 140 K to 125 K in (xx) . The differential spectra are shown in the insets. The small temperature difference is due to the first-order phase transition. The first increases of the low-energy intensity is caused by the increase of the low-energy magnetic fluctuation [15]. The following abrupt decrease is due to the opening of the SDW gap. It should be noted that the full gap does not open as known from the metallic properties in the SDW state. Ran *et al.* [8] calculated that the hole pocket at Γ and the electron pocket folded into Γ make a pseudo-gap with two connecting points by the Dirac nodes. The connecting points are a little above the Fermi level and two small hole pockets are made. Similarly the electron pocket at $(0, \pi)$ and the hole pocket folded into $(0, \pi)$ make a pseudo-gap and two small electron pockets. The gap energy is about 400 cm^{-1} , when it is assigned to the starting point of the deviation between the spectra above and below T_{SDW} . This is the lowest-energy pseudo-gap. The gap structure is not observed in the (aa) and (xy) spectra. Therefore the gap symmetry is B_{2g} . It is the same as the superconducting gap in $\text{BaFe}_{2-x}\text{Co}_x\text{As}_2$ [24, 25]. The hole pocket gives the largest contribution to the electronic scattering intensity in the (aa) spectra, when it is calculated from the $|\partial^2 E / \partial k_i \partial k_s|^2$, where k_i and k_s are the wave vectors in the incident and scattered polarization directions. The reason that the gap does not appear in (aa) is the multi-orbital effect. The total symmetry of the paired state is given by the symmetries in the orbital combination and the momentum space. The observed gap symmetry is given by the B_{2g} symmetry in the orbital combination and the A_{1g} symmetry in the momentum space. The details are presented separately [25].

The sharp peaks at 181 cm^{-1} (A_{1g}) and 215 cm^{-1} (B_{1g}) are phonon peaks [20–23]. Below T_{SDW} the 187 cm^{-1} A_{1g} phonon peak appears in the (ab) spectra. In this polarization configuration the forbidden A_{1g} phonon in the tetragonal structure becomes allowed in the orthorhombic structure, but the intensity is expected to be small because it is proportional to $|R_{11} - R_{22}|^2$ with $R_{11} \approx R_{22}$ using the Raman tensor of the A_{1g} phonon. The intensities in the (aa) and (xx) spectra are proportional to $\frac{1}{4}|R_{11} + R_{22}|^2$ and $|R_{11}|^2$ (or $|R_{22}|^2$), respectively. Both intensities are expected to be close to each other as $R_{11} \approx R_{22}$ and the twinning are expected. Instead at 10 K the intensities in the (xx) and (ab) spectra in which the SDW gap opens are 1.5 ~ 2 times as large as the intensity in (aa) in which the gap closes. This phonon is the mode in which As atom moves in the c direction [20]. It has large magneto-phonon interaction, because the Fe-As-Fe angle is very sensitive to the Fe-Fe exchange interaction energy [26–28]. The detailed mechanism of the enhancement is still an open question. The enhancement of the A_{1g} phonon below T_{SDW} was reported in CaFe_2As_2 [22] and $\text{Ba}(\text{Fe}_{1-x}\text{Co}_x)_2\text{As}_2$ [23]. Similar enhancement of the

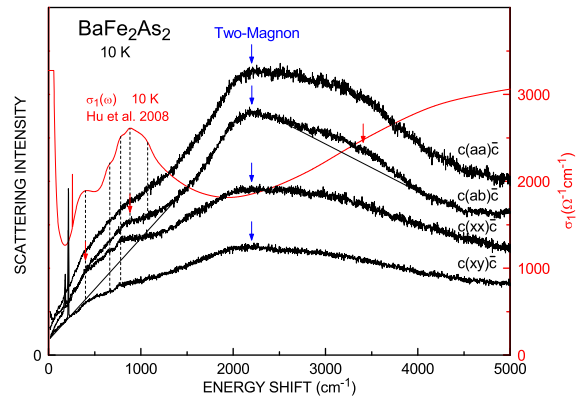


FIG. 2: (color online) Comparison between Raman spectra and optical conductivity at 10 K [9].

infrared active phonon was reported in BaFe_2As_2 [29]

Figure 2 shows the 10 K spectra at various polarization configurations and the optical conductivity at 10 K obtained by Hu *et al.* [9]. The temperature dependence of the Raman spectra are shown in Fig. 3(a). The humps below 1000 cm^{-1} and $2800\text{--}3800 \text{ cm}^{-1}$ disappear above T_{SDW} . Therefore these humps are made by the electronic transition in the reconstructed electronic states created by the folding of the electron pockets and the hole pockets below T_{SDW} . The new broad humps at $400, 900,$ and 3500 cm^{-1} correspond to the $360, 890,$ and 5000 cm^{-1} humps observed in the optical conductivity [9]. The 662 and 780 peaks in the (xx) and (xy) spectra and the 882 and 1072 peaks in the (aa) and (ab) spectra correspond to the fine structure in the optical conductivity spectra [9]. The energy difference 118 cm^{-1} in the former set is close to the E_g phonon energy 117 cm^{-1} and the energy difference 190 cm^{-1} in the latter set is close to the A_{1g} phonon energy 182 cm^{-1} [21]. Very recently Yi *et al.* [11] reported the ARPES results that the electronic structures are significantly reconstructed in the SDW state and cannot be described in the simple folding scenario.

The broad 2200 cm^{-1} (at 10 K) peak is the two-magnon scattering peak. Till now two-magnon scattering is interpreted by the Coulomb interaction induced S^+S^- excitations on the spin waves at k and $-k$. This process expresses two-magnon scattering in the antiferromagnetic (AF) insulator. However, it is noted that BaFe_2As_2 is metal even in the SDW state. We first discuss the two-magnon peak by the Coulomb interaction induced mechanism and then discuss the new carrier induced mechanism by comparing with the cuprate superconductors.

The exchange interaction energies are very different whether the calculation starts from the long-range AF stripe spin structure or from the short-range superexchange interaction. In the former case the exchange interaction energies are obtained from $J_{ij}(R) =$

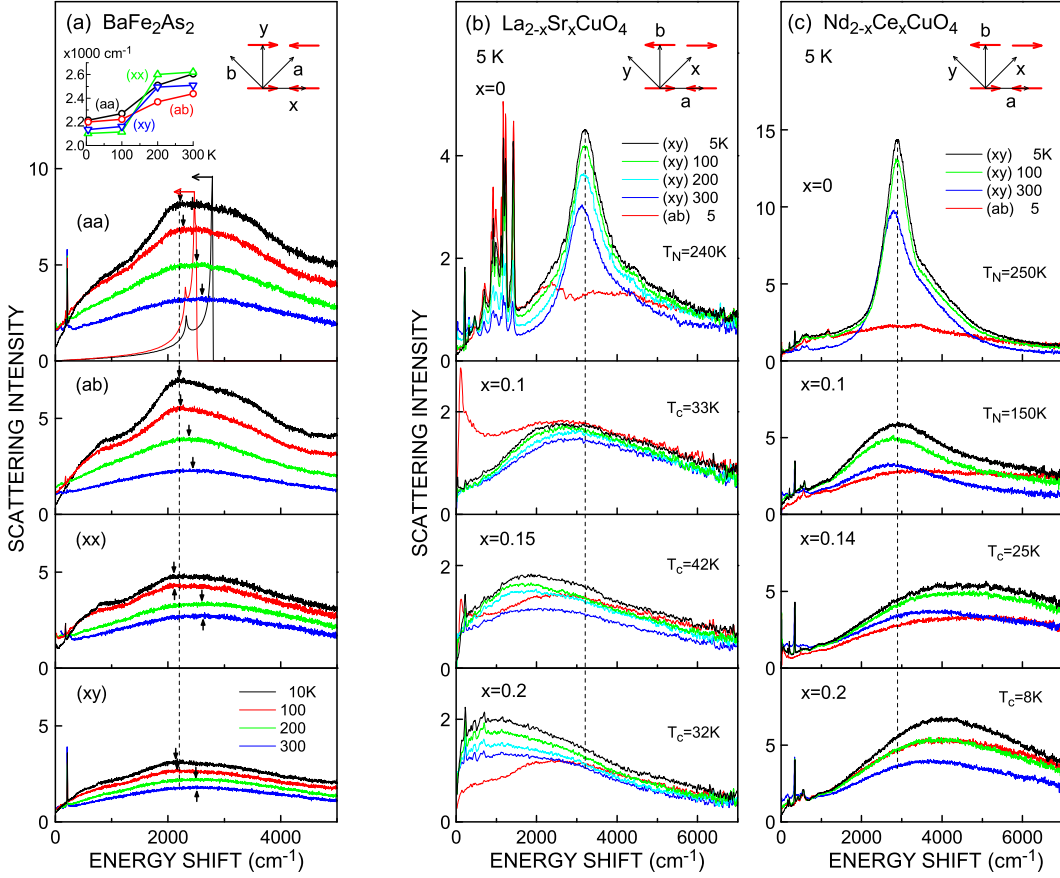


FIG. 3: (color online) (a) Temperature dependent polarized Raman spectra in BaFe_2As_2 . The two-magnon peak is shown by the dashed line. The densities of states for the independent two spin wave excitations are shown with $SJ_{1a} = 36$, $SJ_{1b} = -7.2$, and $SJ_2 = 18$ meV [12] (black) and $SJ_{1a} = 43$, $SJ_{1b} = -3.1$, and $SJ_2 = 14.3$ meV [30] (red) in the (aa) spectra. The two-magnon peak energy is reduced by the magnon-magnon interaction energy as shown by the left-pointing arrows. The inset is the two-magnon peak energy. (b) Two-magnon Raman spectra in hole-doped LSCO and (c) electron-doped NCCO. Two-magnon scattering in the insulating phase is allowed in the (xy) and (aa) spectra, but not in (ab) and (xx) . The low-energy peaks in LSCO with $x = 0.1$ and 0.15 in the (ab) spectra are superconducting coherent peaks.

$-\partial^2 E / \partial \theta_i(0) \partial \theta_j(R)$, where E is the total energy and $\theta_j(R)$ is the angle of the moment of the j th spin [27, 30]. The calculated energies are AF $SJ_{1x} = 43$, ferromagnetic $SJ_{1y} = -3.1$, and AF diagonal $SJ_2 = 14.3$ meV [30]. The low-energy spin wave in the SDW state was observed by neutron scattering in BaFe_2As_2 [12, 15], SrFe_2As_2 [13] and CaFe_2As_2 [14]. Ewings *et al.* [12] fitted the velocity at 7 K in BaFe_2As_2 by the long-range exchange interaction model with $SJ_{1x} = 36$, $SJ_{1y} = -7.2$, and $SJ_2 = 18$ meV. Recent high energy neutron scattering experiment showed that the entire spin wave dispersion of CaFe_2As_2 ($T_N \sim 170$ K) at 10 K is expressed by the long-range model [16]. On the other hand the calculation of the local superexchange interaction gives AF exchange interaction energies for all directions reflecting the equivalent x and y directions. The stripe spin order is stable if $J_{1x} = J_{1y} < 2J_2$, otherwise the checkerboard spin order is stable [26, 31]. The two-magnon peak is observed even

above T_{SDW} in Fig. 3(a), indicating that the short-range spin correlation remains. The $J_{1x} = J_{1y}$ type of exchange interactions may appear above T_{SDW} .

The densities of states of the spin waves calculated using the exchange interaction energies of the first principle calculation (red) and the neutron scattering (black) are shown in the (aa) spectra of Fig. 3(a). The energies are doubled to present independent two magnon excitations. The observed two-magnon peak energy is reduced by the magnon-magnon interaction energy of about J_{1x} as shown by the left-pointing arrow assuming $S = 1$. The calculated two-magnon energy is close to the experimentally obtained two-magnon peak energy.

The two-magnon scattering Hamiltonian is [32]

$$H' = A \sum_{i,j} (\hat{E}_s \cdot \hat{\rho}_{ij})(\hat{E}_i \cdot \hat{\rho}_{ij})(\mathbf{S}_i \cdot \mathbf{S}_j), \quad (1)$$

where $\hat{\rho}_{ij}$ is the unit vector connecting near spins on the

different spin sublattices. From this Hamiltonian two-magnon scattering is active in all polarization configurations in contrast to the cuprate in which the active polarizations are (aa) and (xy) . The difference comes from the large diagonal exchange interaction energy in BaFe_2As_2 .

The very broad two-magnon peak in BaFe_2As_2 is caused by itinerant carriers. The hole density is 0.081 and the electron density is 0.069 per iron atom at 140 K [33]. Figure 3(b) and (c) show the doping dependence in hole-doped $\text{La}_{2-x}\text{Sr}_x\text{CuO}_4$ (LSCO) and electron-doped $\text{Nd}_{2-x}\text{Ce}_x\text{CuO}_4$ (NCCO). The two-magnon peak energy in the (xy) spectra of LSCO decreases with increasing the hole density, whereas it abruptly increases at the insulator-metal transition in NCCO. It is noted that the two-magnon peak is observed above the Néel temperature (T_N) and in the superconducting state, because the short-range correlation remains. Till now the effect of carriers on two-magnon scattering is treated by the Coulomb interaction induced insulating two-magnon scattering process with the reduced AF correlation length. In this model the two-magnon peak decreases in energy and intensity with broadening as the carrier density increases. The increase of the two-magnon peak energy in the metallic phase of NCCO cannot be interpreted. We propose a new model that electronic scattering gives the magnetic excitation component.

A hole or an electron traveling in the antiferromagnetically ordered spin sea leaves behind an changed spin trace, because the carrier spin which hops to the neighboring site is limited by the Pauli principle. The electron Green function representing this state has a self-energy of spin excitations. The electron spectral function that is the imaginary part of the retarded Green function has the coherent component near the original electronic energy and the incoherent component near the spin excitation energy at a fixed k . It is calculated by the string model [34]. The $\Delta k \approx 0$ transition in the electronic Raman scattering detects the magnetic excitations through the incoherent part. The minimum spin excitation is two spin changes of $\Delta S_z = 1$ and $\Delta S_z = -1$ because of the spin conservation with light. The number of changed spins increases and the energy increases as the mean free path of the carrier increases. The mean free path in NCCO is ten times longer than that in LSCO. It causes the high energy shift of the magnetic excitation peak in NCCO. In case of BaFe_2As_2 the observed magnetic excitation peak energy is nearly the same as the calculated two-magnon energy. It indicates that the mean free path is not as long as NCCO and the magnetic correlation length is not as short as LSCO.

The scattering intensity above the maximum of the independent two spin wave excitations comes from the higher order multi-magnon excitations. The higher-order component is much larger in the carrier-induced case than the Coulomb interaction-induced case. The large

higher-order component in BaFe_2As_2 is caused by the carrier-induced process. The mean free path decreases from T_{SDW} to 300 K by 15 %, when it is estimated from the in-plane resistivity. Hence the carrier-induced process does not contribute to increase the higher order multi-magnon scattering. The 2200 cm^{-1} two-magnon peak shifts to $2400 \sim 2600 \text{ cm}^{-1}$ as temperature increases from T_{SDW} to 300 K (inset of Fig. 3(a)). The optical conductivity in the two-magnon energy region and the plasma frequency does not show appreciable change above T_{SDW} [9]. Therefore the high energy shift may be induced by the inclusion of the short-range spin correlation, AF in both x and y .

The present Raman scattering experiment disclosed the anisotropic SDW gap and two-magnon scattering. Two-magnon peak survives far above T_{SDW} indicating the short-range spin correlation remains. The two-magnon scattering process in metal was discussed in comparison with the cuprate superconductors.

This work was supported by Transformative Research Project on Iron Pnictides (TRIP), Japan Science and Technology Agency (JST).

-
- [1] Y. Kamihara, T. Watanabe, M. Hirano, and H. Hosono, *J. Am. Chem. Soc.* **130**, 3296-3297 (2008).
 - [2] Z.-A. Ren *et al.* *Europhys. Lett.* **83**, 17002 (2008).
 - [3] I. I. Mazin, D. J. Singh, M. D. Johannes, and M. H. Du, *Phys. Rev. Lett.* **101**, 057003 (2008).
 - [4] K. Kuroki *et al.* *Phys. Rev. Lett.* **101**, 087004 (2008).
 - [5] J. Dong *et al.* *Europhys. Lett.* **83**, 27006 (2008).
 - [6] H. Ding *et al.* *Europhys. Lett.* **83**, 47001 (2008).
 - [7] K. Terashima *et al.* *Proceedings of the National Academy of Sciences of the United States of America*, **106**, No. 18, 7330 (2009).
 - [8] Y. Ran, F. Wang, H. Zhai, A. Vishwanath, and D.-H. Lee, *Phys. Rev. B* **79**, 014505 (2009).
 - [9] W. Z. Hu *et al.* *Phys. Rev. Lett.* **101**, 257005 (2008).
 - [10] D. Hsieh *et al.* *arXiv:0812.2289v1* (2008),
 - [11] M. Yi *et al.* *arXiv:0909.0831v1*.
 - [12] R. A. Ewings *et al.* *Phys. Rev. B* **78**, 220501(R) (2008).
 - [13] J. Zhao *et al.* *Phys. Rev. Lett.* **101**, 167203 (2008).
 - [14] R. J. McQueeney *et al.* *Phys. Rev. Lett.* **101**, 227205 (2008).
 - [15] K. Matan, R. Morinaga, K. Iida, and T. J. Sato, *Phys. Rev. B* **79**, 054526 (2009).
 - [16] J. Zhao *et al.* *Nature Phys.* **5**, 555 (2009).
 - [17] M. Rotter *et al.* *Phys. Rev. B* **78**, 020503(R) (2008).
 - [18] Q. Huang *et al.* *Phys. Rev. Lett.* **101**, 257003 (2008).
 - [19] C. de la Cruz *et al.* *Nature*, **453**, 899 (2008).
 - [20] A. P. Litvinchuk *et al.* *Phys. Rev. B* **78**, 060503(R) (2008).
 - [21] M. Rahlenbeck *et al.* *Phys. Rev. B* **80**, 064509 (2009).
 - [22] K.-Y. Choi *et al.* *Phys. Rev. B* **78**, 212503 (2008).
 - [23] L. Chauvière *et al.* *Phys. Rev. B* **80**, 094504 (2009).
 - [24] B. Muschler *et al.*, *Phys. Rev. B* **80**, 180510(R) (2009).
 - [25] S. Sugai *et al.* submitted to *Phys. Rev. B*.
 - [26] T. Yildirim, *Phys. Rev. Lett.* **101**, 057010 (2008),

- [27] Z. P. Yin *et al.* Phys. Rev. Lett. **101**, 047001 (2008),
- [28] K. Kuroki, H. Usui, S. Onari, R. Arita, and H. Aoki, Phys. Rev. B **79**, 224511 (2009).
- [29] A. Akrap *et al.* Phys. Rev. B **80**,180502(R) (2009).
- [30] M. J. Han, Q. Yin, W. E. Pickett, and S. Y. Savrasov, Phys. Rev. Lett. **102**, 107003 (2009).
- [31] Q. Si and E. Abrahams, Phys. Rev. Lett. **101**, 076401 (2008),
- [32] J. B. Parkinson, J. Phys. C **2**, 2012 (1969).
- [33] M. Yi *et al.* Phys. Rev. B **80**, 024515 (2009).
- [34] E. Manousakis, Phys. Rev. B **75**, 035106 (2007).